Insulin Sensing by Astrocytes Is Critical for Normal Thermogenesis and Body Temperature Regulation

Iyad H. Manaserh[1,2], **Emily Maly**[1], **Marziyeh Jahromi**[1], **Lakshmikanth Chikkamenahalli**[1], **Joshua Park**[3], **Jennifer Hill**[1,2]

[1]Department of Physiology and Pharmacology, College of Medicine and Life Sciences, The University of Toledo, Toledo, OH 43614

[2]Center for Diabetes and Endocrine Research, College of Medicine and Life Sciences, The University of Toledo, Toledo, OH 43614

[3]Department of Neuroscience, College of Medicine and Life Sciences, The University of Toledo, Ohio 43614

Abstract

The important role of astrocytes in the central control of energy balance and glucose homeostasis has recently been recognized. Changes in thermoregulation can lead to metabolic dysregulation, but the role of astrocytes in this process is not yet clear. Therefore, we generated mice congenitally lacking insulin receptors (IR) in astrocytes (IRKO[GFAP] mice) to investigate the involvement of astrocyte insulin signaling. IRKO[GFAP] mice displayed significantly lower energy expenditure and a strikingly lower basal and fasting body temperature. When exposed to cold, however, they were able to mount a thermogenic response. IRKO[GFAP] mice displayed sex differences in metabolic function and thermogenesis that may contribute to the development of obesity and type II diabetes as early as two months of age. While brown adipose tissue exhibited higher adipocyte size in both sexes, more apoptosis was seen in IRKO[GFAP] males. Less innervation and lower βAR3 expression levels were also observed in IRKO[GFAP] brown adipose tissue. These effects have not been reported in models of astrocyte IR deletion in adulthood. In contrast, body weight and glucose regulatory defects phenocopied such models. These findings identify a novel role for astrocyte insulin signaling in the development of normal body temperature control and sympathetic activation of BAT. Targeting insulin signaling in astrocytes has the potential to serve as a novel target for increasing energy expenditure.

Keywords

Address correspondence to: Jennifer W. Hill, Ph.D.; Dept. of Physiology and Pharmacology, U of Toledo College of Medicine and Life Sciences, 3000 Arlington Ave, MS 1008, Toledo, OH 43614; Tel: (419) 383 6137; Fax: (419) 383 2871; JenniferW.Hill@utoledo.edu.

Conflicts of Interest: None declared

Introduction

Neuronal circuits are influenced by surrounding astrocytes, critical members of the "tripartite synapse" (Araque et al., 1999). Astrocytes exchange information with neurons, respond to synaptic activity, and regulate synaptic transmission through the release of gliotransmitters such as prostaglandins (Xu et al., 2003, Shiow et al., 2017, Perea et al., 2009). Mounting evidence demonstrates the essential role of astrocytes in modulating homeostatic functions including body weight and glucose metabolism. Astrocytes that regulate hypothalamic metabolic circuits act as sensors to inhibit or promote food intake (Kim et al., 2014, Yang et al., 2015). Astrocyte signaling activation within the basal medial hypothalamus, for example, reduces the activity of agouti-related protein (AgRP)-positive neurons and therefore diminishes both basal and ghrelin-induced calorie intake (Yang et al., 2015). Targeting hypothalamic astrocytes with the marker glial fibrillary acidic protein (GFAP) demonstrates that astrocyte insulin signaling plays a role in the transport of glucose into the brain, and thereby helps to suppress food intake during peripheral hyperglycemia (Garcia-Caceres et al., 2016). In addition, impaired leptin signaling in GFAP-positive astrocytes induces gliosis, increases food intake, and promotes obesity (Garcia-Caceres et al., 2016, Kim et al., 2014, Wang et al., 2015).

Energy expenditure through activity and heat generation is an important component of body weight regulation. Provided they have a sufficient caloric supply, mammals are able to maintain their body temperature in a cold environment by vasoconstriction to avoid heat loss from the extremities and by shivering to generate heat from skeletal muscles (Contreras et al., 2015). In addition, the activation of brown adipose tissue (BAT) generates heat through uncoupling protein-1 (UCP1), which uncouples the mitochondrial proton gradient to release energy in a process called adaptive or nonshivering thermogenesis (Oelkrug et al., 2015). The sympathetic nervous system (SNS) plays a large role in this process. The SNS activates BAT β3-adrenergic receptors causing higher UCP1 activity and UCP1 gene expression while increasing lipolysis in white adipose tissue (WAT) (Heeren and Munzberg, 2013). In human infants, the supraclavicular fat depots resemble canonical BAT observed in rodents (Lidell et al., 2013), but there is less BAT in adults and its cellular composition is more heterogeneous (Lidell et al., 2013). In addition to brown adipocytes, adult humans have *UCP1*-expressing "beige" adipocytes interspersed in WAT (Chechi et al., 2017, Harms and Seale, 2013, Schulz et al., 2011). BAT and beige adipose tissues are activated by cold exposure, by high fat diets, and after meal consumption (Vosselman et al., 2013), a phenomenon known as postprandial thermogenesis.

Changes in thermoregulation can result in dysregulation of the systemic metabolism (Heeren and Munzberg, 2013). Indeed, mice with genetic deletion of UCP-1 exhibit obesity in the absence of thermal stress (Feldmann et al., 2009). BAT in adult humans also plays an important role in energy regulation and could be a potential target for the treatment of obesity (Lee et al., 2014, Virtanen et al., 2009). While the involvement of astrocytes in circuits that control energy intake is clear, little information is available on how astrocytes influence the activation of brown and beige adipose tissue. We therefore examined how rendering astrocytes insensitive to insulin might alter thermoregulation in response to metabolic and environmental challenges.

Material and Methods

Animal and Genotyping

To create an astrocyte-specific deletion of IR (IRKO^{GFAP} mice), GFAP-Cre mice (C57Bl/J6) (Frederick National Laboratory for Cancer Research, Frederick, Maryland, United States) were crossed with IR^{loxp} mice (C57Bl/J6) in which exon 4 of the IR gene was flanked by loxP sites (Konner et al., 2007). GFAP is the main intermediate filament protein mature astrocytes and an important component of the cytoskeleton in astrocytes during development (Reeves et al., 1989). After GFAP-Cre homozygous IR floxed mice were generated, we then paired them with homozygous IR floxed carrying the tdTomato gene inserted into the Gt(ROSA)26Sor locus to serve as a reporter under the control of Cre recombinase expression (JAX # 007909). This breeding scheme generated our control (lacking Cre) and experimental mice. IR^{loxp} mice littermates lacking cre expression or GFAP-cre mice were used as controls; comparisons between IR^{loxp} mice and GFAP-Cre mice were also performed where specified. Mice were weaned on postnatal day (PND) 21 and genotyped by real-time PCR performed by Transnetyx, Inc. (Cordova, Tennessee). Mice were maintained on a 12-hour light/dark cycle at 22°C-24°C by the University of Toledo Department of Laboratory Animal Resources. All procedures were approved by the Institutional Animal Care and Use Committee (IACUC) of the University of Toledo College of Medicine and Life Sciences in Toledo, Ohio. All experiments were performed in accord with the relevant guidelines and regulations described in the IACUC-approved protocol number 106448.

Body Composition

Body weights of singly housed mice were measured bi-monthly from 1 to 9 months of age for IR^{loxp} and IR^{GFAP} groups, and weekly from 3–10 weeks for IR^{loxp} and Cre control groups. Body composition was measured at 2 and 7 months of age using nuclear magnetic resonance (NMR) (minispec mq7.5;BurkerOptics, Billerica, Massachusetts).

Glucose and Insulin Tolerance Tests

GTTs and ITTs were performed as previously described (Heinrich et al., 2016). For GTTs, 2 month old mice were fasted for 6 hours and then given a dextrose injection (2g/kg intraperitoneal (IP)). Tail blood glucose was then measured using a glucometer (AlphaTRAK; Abbot Laboratories, Abbott Park, Illinois) at 0, 15, 30, 45, 60, 90 and 120 minutes after injection. For ITTs, mice were fasted for 3–4 hours and then injected with recombinant insulin (0.75U/kg IP). Tail blood glucose was measured at the same time points as the GTT. GTT and ITT testing was repeated at 7 months of age. For quantitative analysis, area under curve (AUC) measurements were calculated for each animal in the control and experimental groups.

Homeostasis Model Assessment of Insulin Resistance (HOMA IR)

At 7–8 months of age, fasting serum was collected, glucose levels were recorded, and insulin levels were measured using an ELISA kit with intra-assay precision CV   10.0% (Crystal Chem, Cat# 90080) and sensitivity of 0.05 ng/ml. The HOMA IR was calculated [fasting

serum glucose × fasting serum insulin/22.5] to assess insulin resistance (Fraulob et al., 2010).

Tissue Collection

Mice were terminated via an IP ketamine/xylazine injection to induce deep anesthesia followed by exsanguination. Liver, gonadal WAT, and interscapular BAT were then collected for gene expression and immunohistochemical staining. For liver and interscapular brown adipose histology, 7–8 months old mice (liver staining) or 9 month old mice (interscapular brown adipose staining) were perfused with 10% formalin after ketamine/xylazine injection. Tissues were post-fixed overnight and then transferred to 70% ETOH until sectioning.

Liver Histology

Liver tissue was paraffin embedded, sectioned, and stained with H&E (Qiu et al., 2013) and ORO (Mehlem et al., 2013). An Olympus BX61US microscope (X-cite 120 LED boost EXCELITAS technology) with OlyVia 2.9 software was used to visualize the staining. Liver sections were analyzed by evaluating lipid accumulation and inflammation via fat droplet counts and inflammatory gene expression levels. Liver sections were automatically analyzed by evaluating the number of fat droplets via ImageJ software (size (pixel^2) was set to 50-infinity, and circularity was set from 0.2–1.00).

Polymerase Chain Reaction (PCR) gel electrophoresis

DNA was extracted from control and experimental groups, using the QIAamp DNA Kit (Cat #: 51304) for 25mg of each tissue sample. PCR was performed for the insulin receptor (IR) for all DNA samples using forward (5´ AAATGACGGGGTGAGGGAAC 3´) and reverse (5´ GGCCGTGAAAGTTAAGAGGGG 3´) primers. The PCR reaction was carried out in a 20 μl volume, with 100 ηg extracted DNA, 0.5 μM of each primer, and 2X Hot-Start Taq Mastermix, (Denville's, Thermo Scientific, U.S.A). The temperature profile was one cycle of 95°C for 5 min (primary denaturation), followed by 35 cycles of 95°C for 30 s (denaturation), 60 °C for 30s (annealing), and 72°C for 40 s (extension), and a final extension 72°C for 5 min (Mikaeili et al., 2013). The extracted DNAs and PCR products of each the method were loaded on separate 2% TAE agarose gels. The gels contained 0.5 μg/ml ethidium bromide for staining. Electrophoresis was carried out for 90 minutes at 80 V. The bands were visualized in UV illuminator and digitally photographed.

Gene Expression Analysis

An RNeasy Lipid Tissue Mini Kit (Qiagen, Valencia, California) permitted total RNA extraction. We synthesized single strand cDNA using a high capacity cDNA Reverse Transcription Kit (Applied Biosystems) (Solanki et al., 2017). In brief, mice were sacrificed via lethal ketamine/xylazine injections, and tissues were removed. 100mg of dissected tissues were transferred into 1 ml of Trizol. The samples were then disrupted using a bead homogenizer. Chloroform was added and the samples were vigorously shaken and incubated at room temperature for 5 minutes. A series of centrifugation steps was then performed and purified RNA was collected. RNA sample concentration was measured using a NanoDrop™ One/OneC Microvolume UV-Vis Spectrophotometer (Thermofisher Scientific). cDNA was

synthesized with random primers and reverse transcriptase (Applied Biosystems) using 1 μg of total RNA. cDNA was evaluated with quantitative RTPCR using True Amp SYBR green qPCR Supermix (Applied Biosystems). The relative amount of mRNA was calculated by comparison to the corresponding controls and normalized relative to Glyceraldehyde 3-phosphate dehydrogenase (GAPDH). Data are presented as means ± SE relative to IR^{loxp} controls [relative quantitation (RQ $=2^{-\Delta Ct}$)]. The sequences of the primers used are as follows: TNF-α; (F: CAGGCGGTGCCTATGTCTC; R: CGATCACCCCGAAGTTCAGTAG), IL-10; (F: GCTGGACAACATACTGCTAACC, R: ATT TCC GAT AAG GCT TGG CAA), LXR- α; (F: AAACTGAAGCGGCAAGAAGA; R: GCAGGACTTGAGGAGGTGAG), UCP-1; (F: GGATGGTGAACCCGACAACT, R: AACTCCGGCTGAGAAGATCTTG), βAR3; (F: GGCACAGGAATGCCACTCCAAT, R: AGGAGGGGAAGGTAGAAGGAGAC), CHOP; (F: AAGCCTGGTATGAGGATCTGC; R: TTCCTGGGGATGAGATATAGGTG), Bcl-2 homologous antagonist killer (BAK); (F: GCCCTGTACGTCTACCAGC; R: TGGCGATGTAATGATGCAGTATG), Bcl-XL; (F: GGTGAGTCGGATTGCAAGTT, R: TGGATCCAAGGCTCTAGGTG), GAPDH; (F: AGGTCGGTGTGAACGGATTTG; R: TGTAGACCATGTAGTTGAGGTCA)

Indirect Calorimetry Analysis

7–8 month old mice were placed in calorimetric chambers (CLAMS system, Columbus Instruments, Columbus, OH), acclimated for 2 days, and then recorded for 3 days with free access to food and water as described (Ghadieh et al., 2015). Locomotor and physical activities were detected via an optical beam measuring vertical and horizontal movements. O_2 consumption (VO_2), CO_2 production and energy expenditure were measured every 20 minutes. The bar graphs show indirect calorimetry parameters (VO2, VCO2, RER, etc) over the 72 hour period. In total, there are 864 individual points per group with each individual point representing the value of a 20 minute interval (3 individual points per hour x 72 hours x 4 mice per group = 864). Data is reported as mean ± SEM of light (600–1800 h) and dark (1800–600 h) cycles (Ghadieh et al., 2015).

Body Temperature Assessment

At 9 months of age, body temperature measurements were obtained using a rectal temperature probe thermometer (Thermalert TH.5, Physitemp NJ) between 9:00–10:00am in the light cycle and 9:00–10:00pm in the dark cycle, as described (Chong et al., 2015a). As specified, baseline readings were obtained from mice with ad libitum access to food and water or following a 12–16h overnight fast.

In the acute cold challenge, we fasted mice overnight and then individually caged them with bedding in a 4°C cold room for 80 minutes. Body temperature was recorded every 20 minutes (Chong et al., 2015a) and food was given when the mice were returned to standard temperatures.

BAT Histology and Immunohistochemistry

Paraffin-embedded BAT tissues were sectioned for staining with H&E (Qiu et al., 2013) or a primary antibody; rabbit anti-TH (Abcam, ab112), rabbit anti-beta 3 adrenergic receptor (Abcam, ab94506); and a biotinylated goat anti-rabbit IgG secondary antibody (Vector lab,

BA-1000). Immunohistochemical staining was performed as previously described (Nobili et al., 2017). Sections were photographed using an Olympus BX61US microscope (X-cite 120 LED boost EXCELITAS technology) with OlyVia 2.9 software. For H&E staining, BAT sections were automatically analyzed by evaluating the size and number of fat droplets via ImageJ software. Images were thresholded using the default setting, size (pixel^2) was set from 50-infinity, and circularity was set from 0.2–1.00. For tyrosine hydroxylase (TH) staining, nerve terminals were counted manually at 40× using OLYvia 2.9 software. For beta 3 adrenergic receptor (βAR3) staining, a score was then giving in a range from 1 (lowest βAR3 expression intensity) to 5 (highest expression intensity). For TH staining and beta 3 adrenergic receptor (βAR3) staining, images obtained from olyvia 2.9 software were evaluated in a blinded manner by three qualified scientists.

Statistical Analysis

All values in the text and figures are presented as mean ± SEM of independent experiments for the given n-sizes. Statistical significance was determined by two-way ANOVA with Tukey post-hoc test or three-way ANOVA with repeated measures followed by Tukey post-hoc test. For all statistical tests, a p value of $P<0.05$ was considered significant. Analyses were performed using GraphPad Prism 8 software (Graph Pad).

Results

To create an astrocyte-specific deletion of the IR (IRKO^{GFAP} mice), IR^{loxp} mice were crossed with a mouse line expressing GFAP promotor-driven cre-recombinase (Konner et al., 2007). In mature astroglia, GFAP is the core intermediate filament protein; it is also an important element of their cytoskeleton during development (Reeves et al., 1989, Middeldorp and Hol, 2011). Thus, these mice lack IR in GFAP-expressing cells throughout life. First, we established that the GFAP-cre mouse line alone shows no significant difference in body composition and systemic metabolism when compared to IR^{loxp} mice (Figure S1 B-H). We have previously characterized the specificity of this deletion (Manaserh et al., 2019). Western blotting confirmed lower IR protein levels in the brains of IRKO^{GFAP} mice (Manaserh et al., 2019). When crossed with a cre-dependent tdTomato red fluorescent protein (RFP) reporter line, RPF was observed in IRKO^{GFAP} astrocytes (Manaserh et al., 2019); 94% of GFAP immunopositive cells were found to show RFP staining. However, there was no localization with RFP when neurons were labeled with the neuronal marker NeuN (Manaserh et al., 2019). By using the astrocyte cell surface antigen-1 (ACSA-1) for fluorescence-activated cell sorting (FACS), we isolated astrocytes from IRKO^{GFAP} mice that exhibited substantially lower IR mRNA levels when compared to astrocytes from control animals and non-astrocyte pools of cells (Manaserh et al., 2019). Gene expression of neuronal (MAP-1), tanycytic (Hes-1 and Hes-5), microglia (Cd11b), and endothelial (vWF) markers were also measured in the astrocyte pool isolated by FACS and confirmed the purity and specificity of these astrocytes. To further validate the specificity of our model, we tested IR expression in peripheral tissues related to thermoregulation including liver, BAT, and WAT via PCR (Figure S1 A). Finally, we used magnetic cell sorting to isolate astrocytes expressing the NA+-dependent glutamate transporter (GLT-1). Western blotting of this population demonstrated prostaglandin E$_2$ (PGE$_2$) synthase levels were lower only in

astrocytes from IRKO^{GFAP} mice (Manaserh et al., 2019). Thus, multiple sources of evidence demonstrate that this line of mice exhibit a specific deletion of the IR in astrocytes.

Using this model, we first examined energy balance and glucose regulation. There were no significant differences in mean bodyweight between IRKO^{GFAP} and IR^{lxop} mice at each age considered (Figure S2 A-B). IRKO^{GFAP} and IR^{loxp} groups also showed comparable fat and lean mass percentages at 2 months of age, but higher fat mass and lower lean mass percentages were observed in IRKO^{GFAP} females at 7 months of age (Figure S2 C-D). Insulin tolerance testing (ITT) revealed sex differences where IRKO^{GFAP} male mice developed insulin resistance starting as early as 2 months. Insulin resistance was also confirmed at 7 months of age in IRKO^{GFAP} male mice (Figure 1 A-C). Unlike males, congenital deletion of astrocyte IR in female mice led to glucose intolerance at 7 months of age (Figure 1 D-F). In contrast, we found that the GFAP-cre only mouse line has a phenotype similar to IR^{loxp} mice (Figure S1 E-H). IRKO^{GFAP} mice exhibited comparable fasting insulin and glucose levels at 7–8 months of age (Figure S3 A-C).

At 7–8 months of age, IRKO^{GFAP} mice showed comparable locomotion and food intake to control animals (Figure S4 A-G). Interestingly, more lipid droplets were seen in their livers (Figure 2 A-B, F) along with higher pro-inflammatory TNF-α gene expression in IRKO^{GFAP} females, lower anti-inflammatory IL-10 mRNA in IRKO^{GFAP} males, and comparable expression of the cholesterol transport marker LXR-α gene in the liver of both sexes (Figure 2 C-E). Notably, IRKO^{GFAP} female mice also displayed lower O_2 consumption (VO_2) (Figure 3 A-B) and had an elevated respiratory exchange ratio (RER), indicating that they utilize less fat for energy production (Figure 3 E). Unlike females, IRKO^{GFAP} male mice exhibited lower VO2, CO_2 production (VCO_2) and RER compared to controls (Figure 3 A-E).

The energy expenditure of male IRKO^{GFAP} mice was lower in IRKO^{GFAP} males (Figure 4 A-B), suggesting less thermogenesis. Indeed, in the fed state, IRKO^{GFAP} mice exhibited lower body temperature in the dark phase (female 33.62 ± 0.2662, male 33.18 ± 0.2418) when compared to the IR^{loxp} group (female 36.76 ± 0.1647, male 36.61 ± 0.2029) (Figure 4 C). After an overnight fast, IRKO^{GFAP} mice displayed a substantially lower body temperature in the light phase (female 32.92 ± 0.4120, male 32.61 ± 0.1184) when compared to controls (female 35.88 ± 0.2833, male 34.66 ± 0.2534) (Figure 4 D). We next tested whether IRKO^{GFAP} mice were able to defend their body temperature during an acute cold temperature challenge. Although IRKO^{GFAP} mice exhibited a lower body temperature at 0 and 20 minutes, body temperatures at 40, 60 and 80 minutes of the cold challenge did not differ from controls. (Figure 4 E)

IRKO^{GFAP} female mice showed larger fat droplets and a lower number of adipocytes in BAT (Figure 5 A, C-D). Similar results were seen in males (Figure 5 B, C-D). IRKO^{GFAP} mice displayed lower UCP-1 mRNA levels in females with a similar trend in males (Figure 6 A), suggesting less SNS outflow. Lower SNS input to BAT may increase apoptosis of adipocytes (Penicaud et al., 2000). Indeed, we found higher pro-apoptotic markers C/EBP Homologous Protein (CHOP) and Bcl-2 homologous antagonist/killer (BAK) mRNA levels (Figure 6 C-

D), and less anti-apoptotic marker B-cell lymphoma-extra-large mRNA (Bcl-XL) in IRKO^{GFAP} female mice (Figure 6 E).

Tyrosine hydroxylase (TH) is a rate limiting enzyme for catecholamine biosynthesis that serves as a marker of denervation (Daubner et al., 2011). IRKO^{GFAP} mice had fewer TH positive nerve endings (119.3 ± 9.735) in BAT when compared to controls (523.3 ± 26.03) (Figure 7 A,C-D). We then determined the levels of β3-adrenergic receptor (βAR3), a G-protein coupled receptor that increases UCP1 levels (Fig. 8). In addition to lower βAR3 mRNA levels in IRKO^{GFAP} females (Figure 6 B), both IRKO^{GFAP} female and male mice had lower protein levels of βAR3 (Figure 8 A-C). These results suggest that insulin resistance in astrocytes alters SNS outflow to BAT. All outlier data points have been included in the main statistical analysis.

Discussion

Maintaining a constant body temperature requires a substantial amount of energy. Therefore, sensing energy availability is a critical function of thermoregulatory circuits. The hormone insulin is one of several metabolic signals that regulate the decision whether to defend a normal body temperature at temperatures below thermoneutrality or to reduce metabolic rate (Humphries et al., 2003, Swoap, 2008). Defense of a chronically lower body temperature set point can conserve energy.

Descending pathways from thermoregulatory centers in the hypothalamus and hindbrain regulate sympathetic neural outflow to BAT to control heat production. The median preoptic nucleus (MnPO) and the medial preoptic area (POA), containing warm-sensitive neurons, were originally recognized as playing a critical role for eliciting fever (Cooper et al., 1967, Lazarus et al., 2007, Morrison et al., 2008, Nakamura and Morrison, 2008, Romanovsky et al., 2009). They have reciprocal connections with the OVLT, a structure at the anterior wall of the third ventricle that senses circulating pyrogens (Ott et al., 2010, Blatteis, 1992). Neurons in the preoptic hypothalamus are believed to provide a tonic inhibitory GABAergic input to thermogenic pre-sympathetic neurons in the rostral medullary raphe nucleus (RMR) of the brain stem. In addition to the direct inhibitory projection from the preoptic hypothalamus to the RMR, this structure also receives input from the preoptic hypothalamus via a relay in the dorsomedial hypothalamus (DMH). The input from the DMH is excitatory, though still under inhibitory control from the preoptic hypothalamus (Nakamura et al., 2005). The DMH is a critical node for cold induced thermogenesis (Almeida et al., 2006); thermogenesis through sympathetic activation of BAT requires the disinhibition of the projection to the RMR from the DMH (Rathner et al., 2008). Shivering thermogenesis may also be mediated by this pathway (Nakamura and Morrison, 2011). Other hypothalamic regions, including the VMH, LHA, PVH, and arcuate (via projections to the PVH) also modify the sympathetic activation of thermogenesis in BAT and BeAT (Fuller et al., 1975, Holt et al., 1987, Contreras et al., 2017, Lage et al., 2016, Amir and Schiavetto, 1990, Monda et al., 1997).

Insulin is known to play a role in the neuronal control of body temperature (Sanchez-Alavez et al., 2010, Chong et al., 2015a). Insulin can cause hyperthermia by direct inhibition of

warm-sensitive neurons in the POA (Sanchez-Alavez et al., 2010). However, a role for astrocyte insulin sensing has not been previously identified. Previous work has shown that insulin signaling in astrocytes regulates GLUT-1 expression, the number and/or length of astrocyte processes throughout the brain, and the activation and synaptic contacts of neurons in the arcuate nucleus (Garcia-Caceres et al., 2016, Salameh et al., 2016). In addition, insulin signaling in astrocytes has been shown to increase exocytosis of ATP from astrocytes, which can alter the function of adjacent neurons (Cai et al., 2018). Through such means, insulin responsive astrocytes in the vicinity of thermogenic circuits may help those neurons respond in a metabolically appropriate manner.

In IRKO^{GFAP} mice, regulation of basal body temperature was disturbed when the mice were awake, the time period during which feeding and other activity occurs. The drop of body temperature during their period of highest physical activity is surprising. Insulin is known to affect postprandial thermogenesis; intranasal insulin administration in humans enhances the acute thermoregulatory response to food intake (Benedict et al., 2011). However, the basal body temperature of IRKO^{GFAP} mice was 1–2 degrees lower under the dark phase in fed conditions as well as overnight fasted conditions. The latter finding argues against an alteration in postprandial heat generation accounting for the difference in temperature.

It is also possible that insulin action in astrocytes of the blood-brain barrier underlies the alteration in body temperature in this model. Others have demonstrated a lower availability of glucose to hypothalamic neurons in IRKO^{GFAP} mice due to reduced glucose transport into the brain (Cai et al., 2018)(Garcia-Caceres et al., 2016). Increased glucose demand by neurons in the awake animal (Thomas et al., 2000) may result in insufficient local glucose availability to hypothalamic neurons for efficient body temperature regulation. If so, one would expect that mouse lines lacking astrocyte IR expression only in adulthood would share this phenotype. While body temperature does not appear to have been directly measured in such mice, they reportedly show normal energy expenditure (Cai et al., 2018), contrary to predictions if body heat were affected. The contrasting finding of lower energy expenditure in IRKO^{GFAP} male mice in the current study suggests that the absence of insulin signaling in astrocytes during development leads to altered body temperature circuitry. Neuronal insulin signaling can influence neuronal survival (Mielke et al., 2006, Valenciano et al., 2006), dendritic outgrowth and arbor development (Govind et al., 2001, Cheng et al., 2003), and the maintenance of synapses (Chiu and Cline, 2010). Several IR signaling pathways have been implicated in excitatory synaptic connectivity and dendritic structure (Wu et al., 2001, Dunah et al., 2005). Whether these processes are also modulated by insulin sensing by astrocytes is unclear but deserves attention.

Given the lack of an effect of astrocytic IR signaling on total body weight, it is unsurprising that chronic absence of astrocyte insulin signaling driven by congenital expression of hGFAP-cre caused no change in body composition, locomotor activity, or food intake at 2 months of age. However, sex differences in systemic metabolism were notable. While IRKO^{GFAP} male mice demonstrated insulin resistance at 2 months and 7 months of age, IRKO^{GFAP} females did not. Instead, IRKO^{GFAP} females exhibited a higher fat mass (%) and lower lean mass (%) at 7 months of age, accompanied by glucose intolerance. These findings suggest that these metabolic effects of insulin signaling in astrocytes are solely due

to effects in the adult brain. Indeed, adult deletion of IR in GFAP-expressing cells altered astrocytic morphology and circuit connectivity (Garcia-Caceres et al., 2016).

Despite a lower basal body temperature, IRKO^{GFAP} mice exhibited a normal increase in temperature when exposed to a major cold challenge. Astrocyte populations that respond to metabolic factors are likely distinct from those involved in responding to cold conditions, similar to recent findings regarding insulin-sensing neurons. When insulin and leptin receptors are deleted from Nkx2.1-positive neurons of the hypothalamus and basal ganglia, mice expend less energy, resulting in higher body weight and adiposity (Chong et al., 2015b). These double knockout mice also exhibited a 1.5°C lower core body temperature during the fed state when housed at 20–22°C, a mild cold stress. Further, these mice dramatically reduce their body temperature during a fast (Chong et al., 2015a, Chong et al., 2015b). At 4°C, however, fasted mice were able to quickly increase their body temperature (Chong et al., 2015b). Neurons in the midbrain and brainstem that form polysynaptic connections with BAT may be sufficient to maintain a thermogenic response to an acute cold challenge (Hermann et al., 2006, Nautiyal et al., 2008). These brain regions may differentially regulate sympathetic outflow to WAT and BAT in response to fasting and cold exposure (Brito et al., 2008, Murano et al., 2009, Bamshad et al., 1999, Bamshad et al., 1998). A recent study found a differential sympathetic drive to WAT and BAT for different lipolytic stimuli; for example, fasting altered beiging selectively in subcutaneous WAT without affecting BAT, an effect that was replicated by activation of AgRP neurons in the ARC (Ruan et al., 2014). In contrast, RIP-Cre neurons in VMH regulated WAT beiging and lipolysis preferentially in WAT in response to cold exposure but not fasting (Wang et al., 2018). These studies shed light on how regional neuronal circuits can tailor the modulation of body temperature to the type of stimulus received.

An important caveat for these considerations derives from the limitations of rectal probe measurement of body temperature. This procedure may be uncomfortable for the mice, and stress is known to induce vasoconstriction to maintain core body temperature (Charkoudian, 2010). Repeated probe measurements in the cold challenge may therefore have interfered with the natural response to the low external temperature in both the experimental and control groups. Future experiments should employ intra-BAT and/or intraperitoneal implanted temperature probes to examine longitudinal body temperature regulation without mouse handling.

IRKO^{GFAP} female mice exhibited less VO$_2$ consumption and higher RER, indicating that they utilize less fat for energy homeostasis. In male mice, an RER of around 0.87 for IR^{loxp} and 0.82 for IRKO^{GFAP} shows CO$_2$ production was lowered more than O$_2$ consumption in the IRKO^{GFAP} males. Our model exhibits that less β3-adrenergic receptor and UCP-1 gene expression was seen in IRKO^{GFAP} female BAT, with only a trend towards a reduction in IRKO^{GFAP} males. These findings suggest less SNS outflow, which may increase apoptosis of adipocytes (Penicaud et al., 2000). In accord with this idea, we found that IRKO^{GFAP} mice exhibited fewer adipocytes with bigger fat droplets in BAT. Interestingly, we found sex differences in BAT morphology. While IRKO^{GFAP} females showed lower β3-adrenergic receptor and UCP-1 gene expression, IRKO^{GFAP} males demonstrated higher expression of pro-apoptotic (CHOP and BAK) genes and lower expression of anti-apoptotic (Bcl-XL)

genes. These findings support the idea that astrocyte insulin signaling affects thermogenesis by modulating SNS outflow to BAT.

Several mechanistic questions remain to be explored. Interestingly, the phenotype of IRKO^{GFAP} mice is associated with lower PGE$_2$ synthase in the hypothalamus (Manaserh et al., 2019), which catalyzes the conversion of prostaglandin H2 to PGE$_2$. PGE$_2$, a prostaglandin synthesized by cyclooxygenases (COX), plays a key role in regulating body temperature (Cao et al., 1997, Matsumura et al., 1997, Feleder et al., 2004). Indeed, several studies suggest astrocyte PGE$_2$ production may influence body temperature regulation (Yun et al., 2011, Kageyama et al., 2013) by altering the function of adjacent neurons (Clasadonte et al., 2011). Previous studies in humans have shown that blockade of PGE$_2$ production by COX inhibitors can lead to hypothermia (Donaldson and Keatinge, 1997). Overall, our findings are consistent with central insulin action regulating thermogenesis via astrocyte production of PGE$_2$.

Notably, the POA is the site most sensitive to the pyrogenic action of PGE$_2$ (Scammell et al., 1996a, Scammell et al., 1998) and expresses a high concentration of the PGE$_2$ receptor EP$_3$ (Ek et al., 2000, Oka et al., 2000, Vasilache et al., 2007). Administration of PGE$_2$ into the POA of the monkey resulted in a marked and dose-dependent fever response (Onoe et al., 1992), while PGE$_2$ injection into the POA of rats induced fever and Fos induction in the ventromedial POA and the paraventricular nucleus (PVH) (Scammell et al., 1996b). In mice, low PGE$_2$ levels in the POA can reduce body temperature (Bhatnagar et al., 1993b, Yoshida et al., 2009). Preoptic neurons are silenced when PGE$_2$ binds to EP$_3$ receptors, hence providing a disinhibition of RMR presympathetic neurons. Neurons found in the MnPO are responsive to the action of PGE$_2$ and project directly to the RMR (Yoshida et al., 2009). Skin vasoconstriction due to skin cooling or PGE$_2$ delivery to the preoptic hypothalamus depends on the inhibition of the direct projection from the POA to the RMR. Administration of PGE$_2$ to the PVH also leads to the activation of BAT thermogenesis (Bhatnagar et al., 1993a, Contreras et al., 2017). The POA and PVH are thus prime candidates for further investigation of the role of insulin-sensitive astrocytes in thermogenesis.

In summary, our data confirm that impaired insulin signaling in astrocytes lead to systemic insulin and glucose dysregulation largely due to actions in the adult brain. These studies have demonstrated that astrocyte insulin signaling contributes to body temperature regulation by influencing sympathetic stimulation of heat generation by BAT. It is possible that the lower production of astrocyte PGE$_2$ synthase induced by absence of astrocytic insulin signaling contributes to dysregulation of body temperature in this model. Given that thermogenesis is a critical component of energy expenditure, our results suggest that insulin resistance in astrocytes may contribute to the development of obesity and type 2 diabetes or exacerbate these conditions when already present, providing a potential target for therapeutic strategies.

Supplementary Material

Refer to Web version on PubMed Central for supplementary material.

Acknowledgments

References

ALMEIDA MC, STEINER AA, BRANCO LGS & ROMANOVSKY AA 2006 Neural Substrate of Cold-Seeking Behavior in Endotoxin Shock. Plos One, 1.

AMIR S & SCHIAVETTO A 1990 Injection of prostaglandin E2 into the anterior hypothalamic preoptic area activates brown adipose tissue thermogenesis in the rat. Brain Res, 528, 138–42. [PubMed: 2245331]

ARAQUE A, PARPURA V, SANZGIRI RP & HAYDON PG 1999 Tripartite synapses: glia, the unacknowledged partner. Trends Neurosci, 22, 208–15. [PubMed: 10322493]

BAMSHAD M, AOKI VT, ADKISON MG, WARREN WS & BARTNESS TJ 1998 Central nervous system origins of the sympathetic nervous system outflow to white adipose tissue. Am J Physiol, 275, R291–9. [PubMed: 9688991]

BAMSHAD M, SONG CK & BARTNESS TJ 1999 CNS origins of the sympathetic nervous system outflow to brown adipose tissue. Am J Physiol, 276, R1569–78. [PubMed: 10362733]

BENEDICT C, BREDE S, SCHIOTH HB, LEHNERT H, SCHULTES B, BORN J & HALLSCHMID M 2011 Intranasal insulin enhances postprandial thermogenesis and lowers postprandial serum insulin levels in healthy men. Diabetes, 60, 114–8. [PubMed: 20876713]

BHATNAGAR S, MEANEY MJ & AMIR S 1993a The Effects of Prostaglandin-E(2) Injected into the Paraventricular Nucleus of the Hypothalamus on Brown Adipose-Tissue Thermogenesis in Spontaneously Hypertensive Rats. Brain Research, 613, 285–287. [PubMed: 8186977]

BHATNAGAR S, MEANEY MJ & AMIR S 1993b The effects of prostaglandin E2 injected into the paraventricular nucleus of the hypothalamus on brown adipose tissue thermogenesis in spontaneously hypertensive rats. Brain Res, 613, 285–7. [PubMed: 8186977]

BLATTEIS CM 1992 Role of the Ovlt in the Febrile Response to Circulating Pyrogens. Circumventricular Organs and Brain Fluid Environment : Molecular and Functional Aspects, 91, 409–412.

BRITO NA, BRITO MN & BARTNESS TJ 2008 Differential sympathetic drive to adipose tissues after food deprivation, cold exposure or glucoprivation. Am J Physiol Regul Integr Comp Physiol, 294, R1445–52. [PubMed: 18321949]

CAI W, XUE C, SAKAGUCHI M, KONISHI M, SHIRAZIAN A, FERRIS HA, LI ME, YU R, KLEINRIDDERS A, POTHOS EN et al. 2018 Insulin regulates astrocyte gliotransmission and modulates behavior. J Clin Invest, 128, 2914–2926. [PubMed: 29664737]

CAO C, MATSUMURA K, YAMAGATA K & WATANABE Y 1997 Involvement of cyclooxygenase-2 in LPS-induced fever and regulation of its mRNA by LPS in the rat brain. Am J Physiol, 272, R1712–25. [PubMed: 9227582]

CHARKOUDIAN N 2010 Mechanisms and modifiers of reflex induced cutaneous vasodilation and vasoconstriction in humans. J Appl Physiol (1985), 109, 1221–8. [PubMed: 20448028]

CHECHI K, VOISINE P, MATHIEU P, LAPLANTE M, BONNET S, PICARD F, JOUBERT P & RICHARD D 2017 Functional characterization of the Ucp1-associated oxidative phenotype of human epicardial adipose tissue. Sci Rep, 7, 15566. [PubMed: 29138472]

CHENG CM, MERVIS RF, NIU SL, SALEM N JR., WITTERS LA, TSENG V, REINHARDT R & BONDY CA 2003 Insulin-like growth factor 1 is essential for normal dendritic growth. J Neurosci Res, 73, 1–9. [PubMed: 12815703]

CHIU SL & CLINE HT 2010 Insulin receptor signaling in the development of neuronal structure and function. Neural Dev, 5, 7. [PubMed: 20230616]

CHONG AC, GREENDYK RA & ZELTSER LM 2015a Distinct networks of leptin- and insulin-sensing neurons regulate thermogenic responses to nutritional and cold challenges. Diabetes, 64, 137–46. [PubMed: 25125486]

CHONG ACN, GREENDYK RA & ZELTSER LM 2015b Distinct Networks of Leptin- and Insulin-Sensing Neurons Regulate Thermogenic Responses to Nutritional and Cold Challenges. Diabetes, 64, 137–146. [PubMed: 25125486]

CLASADONTE J, POULAIN P, HANCHATE NK, CORFAS G, OJEDA SR & PREVOT V 2011 Prostaglandin E2 release from astrocytes triggers gonadotropin-releasing hormone (GnRH) neuron firing via EP2 receptor activation. Proc Natl Acad Sci U S A, 108, 16104–9. [PubMed: 21896757]

CONTRERAS C, GONZALEZ F, FERNO J, DIEGUEZ C, RAHMOUNI K, NOGUEIRAS R & LOPEZ M 2015 The brain and brown fat. Ann Med, 47, 150–68. [PubMed: 24915455]

CONTRERAS C, NOGUEIRAS R, DIEGUEZ C, RAHMOUNI K & LOPEZ M 2017 Traveling from the hypothalamus to the adipose tissue: The thermogenic pathway. Redox Biol, 12, 854–863. [PubMed: 28448947]

COOPER KE, CRANSTON WI & HONOUR AJ 1967 Observations on the site & mode of action of pyrogens in the rabbit brain. J Physiol, 191, 325–37. [PubMed: 6050108]

DAUBNER SC, LE T & WANG S 2011 Tyrosine hydroxylase and regulation of dopamine synthesis. Arch Biochem Biophys, 508, 1–12. [PubMed: 21176768]

DONALDSON GC & KEATINGE WR 1997 Mortality related to cold weather in elderly people in southeast England, 1979–94. BMJ, 315, 1055–6. [PubMed: 9366732]

DUNAH AW, HUESKE E, WYSZYNSKI M, HOOGENRAAD CC, JAWORSKI J, PAK DT, SIMONETTA A, LIU G & SHENG M 2005 LAR receptor protein tyrosine phosphatases in the development and maintenance of excitatory synapses. Nat Neurosci, 8, 458–67. [PubMed: 15750591]

EK M, ARIAS C, SAWCHENKO P & ERICSSON-DAHLSTRAND A 2000 Distribution of the EP3 prostaglandin E-2 receptor subtype in the rat brain: Relationship to sites of interleukin-1-induced cellular responsiveness. Journal of Comparative Neurology, 428, 5–19. [PubMed: 11058221]

FELDMANN HM, GOLOZOUBOVA V, CANNON B & NEDERGAARD J 2009 UCP1 ablation induces obesity and abolishes diet-induced thermogenesis in mice exempt from thermal stress by living at thermoneutrality. Cell Metab, 9, 203–9. [PubMed: 19187776]

FELEDER C, PERLIK V & BLATTEIS CM 2004 Preoptic alpha 1- and alpha 2-noradrenergic agonists induce, respectively, PGE2-independent and PGE2-dependent hyperthermic responses in guinea pigs. Am J Physiol Regul Integr Comp Physiol, 286, R1156–66. [PubMed: 14962823]

FRAULOB JC, OGG-DIAMANTINO R, FERNANDES-SANTOS C, AGUILA MB & MANDARIM-DE-LACERDA CA 2010 A Mouse Model of Metabolic Syndrome: Insulin Resistance, Fatty Liver and Non-Alcoholic Fatty Pancreas Disease (NAFPD) in C57BL/6 Mice Fed a High Fat Diet. J Clin Biochem Nutr, 46, 212–23. [PubMed: 20490316]

FULLER CA, HORWITZ BA & HOROWITZ JM 1975 Shivering and nonshivering thermogenic responses of cold-exposed rats to hypothalamic warming. Am J Physiol, 228, 1519–24. [PubMed: 1130555]

GARCIA-CACERES C, QUARTA C, VARELA L, GAO Y, GRUBER T, LEGUTKO B, JASTROCH M, JOHANSSON P, NINKOVIC J, YI CX, et al. 2016 Astrocytic Insulin Signaling Couples Brain Glucose Uptake with Nutrient Availability. Cell, 166, 867–880. [PubMed: 27518562]

GHADIEH HE, SMILEY ZN, KOPFMAN MW, NAJJAR MG, HAKE MJ & NAJJAR SM 2015 Chlorogenic acid/chromium supplement rescues diet-induced insulin resistance and obesity in mice. Nutr Metab (Lond), 12, 19. [PubMed: 26045713]

GOVIND S, KOZMA R, MONFRIES C, LIM L & AHMED S 2001 Cdc42Hs facilitates cytoskeletal reorganization and neurite outgrowth by localizing the 58-kD insulin receptor substrate to filamentous actin. J Cell Biol, 152, 579–94. [PubMed: 11157984]

HARMS M & SEALE P 2013 Brown and beige fat: development, function and therapeutic potential. Nat Med, 19, 1252–63. [PubMed: 24100998]

HEEREN J & MUNZBERG H 2013 Novel aspects of brown adipose tissue biology. Endocrinol Metab Clin North Am, 42, 89–107. [PubMed: 23391242]

HEINRICH G, RUSSO L, CASTANEDA TR, PFEIFFER V, GHADIEH HE, GHANEM SS, WU J, FAULKNER LD, ERGUN S, MCINERNEY MF, et al. 2016 Leptin Resistance Contributes to Obesity in Mice with Null Mutation of Carcinoembryonic Antigen-related Cell Adhesion Molecule 1. J Biol Chem, 291, 11124–32. [PubMed: 27002145]

HERMANN GE, BARNES MJ & ROGERS RC 2006 Leptin and thyrotropin-releasing hormone: cooperative action in the hindbrain to activate brown adipose thermogenesis. Brain Res, 1117, 118–24. [PubMed: 16956588]

HOLT SJ, WHEAL HV & YORK DA 1987 Hypothalamic control of brown adipose tissue in Zucker lean and obese rats. Effect of electrical stimulation of the ventromedial nucleus and other hypothalamic centres. Brain Res, 405, 227–33. [PubMed: 3567603]

HUMPHRIES MM, THOMAS DW & KRAMER DL 2003 The role of energy availability in Mammalian hibernation: a cost-benefit approach. Physiol Biochem Zool, 76, 165–79. [PubMed: 12794670]

KAGEYAMA H, ENDO K, OSAKA T, WATANABE J, WANG LH, ITO K, SUZUKI M, SAKAGAMI J, TAKENOYA F & SHIODA S 2013 Galanin-like peptide (GALP) facilitates thermogenesis via synthesis of prostaglandin E2 by astrocytes in the periventricular zone of the third ventricle. J Mol Neurosci, 50, 443–52. [PubMed: 23354880]

KIM JG, SUYAMA S, KOCH M, JIN S, ARGENTE-ARIZON P, ARGENTE J, LIU ZW, ZIMMER MR, JEONG JK, SZIGETI-BUCK K, et al. 2014 Leptin signaling in astrocytes regulates hypothalamic neuronal circuits and feeding. Nat Neurosci, 17, 908–10. [PubMed: 24880214]

KONNER AC, JANOSCHEK R, PLUM L, JORDAN SD, ROTHER E, MA X, XU C, ENRIORI P, HAMPEL B, BARSH GS, et al. 2007 Insulin action in AgRP-expressing neurons is required for suppression of hepatic glucose production. Cell Metab, 5, 438–49. [PubMed: 17550779]

LAGE R, FERNO J, NOGUEIRAS R, DIEGUEZ C & LOPEZ M 2016 Contribution of adaptive thermogenesis to the hypothalamic regulation of energy balance. Biochem J, 473, 4063–4082. [PubMed: 27834738]

LAZARUS M, YOSHIDA K, COPPARI R, BASS CE, MOCHIZUKI T, LOWELL BB & SAPER CB 2007 EP3 prostaglandin receptors in the median preoptic nucleus are critical for fever responses. Nat Neurosci, 10, 1131–3. [PubMed: 17676060]

LEE P, WERNER CD, KEBEBEW E & CELI FS 2014 Functional thermogenic beige adipogenesis is inducible in human neck fat. Int J Obes (Lond), 38, 170–6. [PubMed: 23736373]

LIDELL ME, BETZ MJ, DAHLQVIST LEINHARD O, HEGLIND M, ELANDER L, SLAWIK M, MUSSACK T, NILSSON D, ROMU T, NUUTILA P, et al. 2013 Evidence for two types of brown adipose tissue in humans. Nat Med, 19, 631–4. [PubMed: 23603813]

MANASERH IH, CHIKKAMENAHALLI L, RAVI S, DUBE PR, PARK JJ & HILL JW 2019 Ablating astrocyte insulin receptors leads to delayed puberty and hypogonadism in mice. PLoS Biol, 17, e3000189. [PubMed: 30893295]

MATSUMURA K, CAO C & WATANABE Y 1997 Possible role of cyclooxygenase-2 in the brain vasculature in febrile response. Ann N Y Acad Sci, 813, 302–6. [PubMed: 9100897]

MEHLEM A, HAGBERG CE, MUHL L, ERIKSSON U & FALKEVALL A 2013 Imaging of neutral lipids by oil red O for analyzing the metabolic status in health and disease. Nat Protoc, 8, 1149–54. [PubMed: 23702831]

MIDDELDORP J & HOL EM 2011 GFAP in health and disease. Prog Neurobiol, 93, 421–43. [PubMed: 21219963]

MIELKE JG, TAGHIBIGLOU C & WANG YT 2006 Endogenous insulin signaling protects cultured neurons from oxygen-glucose deprivation-induced cell death. Neuroscience, 143, 165–73. [PubMed: 16978790]

MIKAEILI F, KIA EB, SHARBATKHORI M, SHARIFDINI M, JALALIZAND N, HEIDARI Z, ZAREI Z, STENSVOLD CR & MIRHENDI H 2013 Comparison of six simple methods for extracting ribosomal and mitochondrial DNA from Toxocara and Toxascaris nematodes. Exp Parasitol, 134, 155–9. [PubMed: 23499880]

MONDA M, SULLO A, DE LUCA V, VIGGIANO A & PELLICANO MP 1997 Acute lesions of the ventromedial hypothalamus reduce sympathetic activation and thermogenic changes induced by PGE1. J Physiol Paris, 91, 285–90. [PubMed: 9457660]

MORRISON SF, NAKAMURA K & MADDEN CJ 2008 Central control of thermogenesis in mammals. Exp Physiol, 93, 773–97. [PubMed: 18469069]

MURANO I, BARBATELLI G, GIORDANO A & CINTI S 2009 Noradrenergic parenchymal nerve fiber branching after cold acclimatisation correlates with brown adipocyte density in mouse adipose organ. J Anat, 214, 171–8. [PubMed: 19018882]

NAKAMURA K & MORRISON SF 2008 A thermosensory pathway that controls body temperature. Nature Neuroscience, 11, 62–71. [PubMed: 18084288]

NAKAMURA K & MORRISON SF 2011 Central efferent pathways for cold-defensive and febrile shivering. J Physiol, 589, 3641–58. [PubMed: 21610139]

NAKAMURA Y, NAKAMURA K, MATSUMURA K, KOBAYASHI S, KANEKO T & MORRISON SF 2005 Direct pyrogenic input from prostaglandin EP3 receptor-expressing preoptic neurons to the dorsomedial hypothalamus. European Journal of Neuroscience, 22, 3137–3146. [PubMed: 16367780]

NAUTIYAL KM, DAILEY M, BRITO N, BRITO MN, HARRIS RB, BARTNESS TJ & GRILL HJ 2008 Energetic responses to cold temperatures in rats lacking forebrain-caudal brain stem connections. Am J Physiol Regul Integr Comp Physiol, 295, R789–98. [PubMed: 18635447]

NOBILI A, LATAGLIATA EC, VISCOMI MT, CAVALLUCCI V, CUTULI D, GIACOVAZZO G, KRASHIA P, RIZZO FR, MARINO R, FEDERICI M, et al. 2017 Dopamine neuronal loss contributes to memory and reward dysfunction in a model of Alzheimer's disease. Nat Commun, 8, 14727. [PubMed: 28367951]

OELKRUG R, POLYMEROPOULOS ET & JASTROCH M 2015 Brown adipose tissue: physiological function and evolutionary significance. J Comp Physiol B, 185, 587–606. [PubMed: 25966796]

OKA T, OKA K, SCAMMELL TE, LEE C, KELLY JF, NANTEL F, ELMQUIST JK & SAPER CB 2000 Relationship of EP(1–4) prostaglandin receptors with rat hypothalamic cell groups involved in lipopolysaccharide fever responses. J Comp Neurol, 428, 20–32. [PubMed: 11058222]

ONOE H, WATANABE Y, ONO K, KOYAMA Y & HAYAISHI O 1992 Prostaglandin-E(2) Exerts an Awakening Effect in the Posterior Hypothalamus at a Site Distinct from That Mediating Its Febrile Action in the Anterior Hypothalamus. Journal of Neuroscience, 12, 2715–2725. [PubMed: 1613554]

OTT D, MURGOTT J, RAFALZIK S, WUCHERT F, SCHMALENBECK B, ROTH J & GERSTBERGER R 2010 Neurons and glial cells of the rat organum vasculosum laminae terminalis directly respond to lipopolysaccharide and pyrogenic cytokines. Brain Research, 1363, 93–106. [PubMed: 20883673]

PENICAUD L, COUSIN B, LELOUP C, LORSIGNOL A & CASTEILLA L 2000 The autonomic nervous system, adipose tissue plasticity, and energy balance. Nutrition, 16, 903–8. [PubMed: 11054595]

PEREA G, NAVARRETE M & ARAQUE A 2009 Tripartite synapses: astrocytes process and control synaptic information. Trends Neurosci, 32, 421–31. [PubMed: 19615761]

QIU X, DOWLING AR, MARINO JS, FAULKNER LD, BRYANT B, BRUNING JC, ELIAS CF & HILL JW 2013 Delayed puberty but normal fertility in mice with selective deletion of insulin receptors from Kiss1 cells. Endocrinology, 154, 1337–48. [PubMed: 23392256]

RATHNER JA, MADDEN CJ & MORRISON SF 2008 Central pathway for spontaneous and prostaglandin E2-evoked cutaneous vasoconstriction. Am J Physiol Regul Integr Comp Physiol, 295, R343–54. [PubMed: 18463193]

REEVES SA, HELMAN LJ, ALLISON A & ISRAEL MA 1989 Molecular cloning and primary structure of human glial fibrillary acidic protein. Proc Natl Acad Sci U S A, 86, 5178–82. [PubMed: 2740350]

ROMANOVSKY AA, ALMEIDA MC, GARAMI A, STEINER AA, NORMAN MH, MORRISON SF, NAKAMURA K, BURMEISTER JJ & NUCCI TB 2009 The Transient Receptor Potential Vanilloid-1 Channel in Thermoregulation: A Thermosensor It Is Not. Pharmacological Reviews, 61, 228–261. [PubMed: 19749171]

RUAN HB, DIETRICH MO, LIU ZW, ZIMMER MR, LI MD, SINGH JP, ZHANG K, YIN R, WU J, HORVATH TL et al. 2014 O-GlcNAc transferase enables AgRP neurons to suppress browning of white fat. Cell, 159, 306–17. [PubMed: 25303527]

SALAMEH TS, SHAH GN, PRICE TO, HAYDEN MR & BANKS WA 2016 Blood-Brain Barrier Disruption and Neurovascular Unit Dysfunction in Diabetic Mice: Protection with the Mitochondrial Carbonic Anhydrase Inhibitor Topiramate. J Pharmacol Exp Ther, 359, 452–459. [PubMed: 27729477]

SANCHEZ-ALAVEZ M, TABAREAN IV, OSBORN O, MITSUKAWA K, SCHAEFER J, DUBINS J, HOLMBERG KH, KLEIN I, KLAUS J, GOMEZ LF, et al. 2010 Insulin causes hyperthermia by direct inhibition of warm-sensitive neurons. Diabetes, 59, 43–50. [PubMed: 19846801]

SCAMMELL TE, ELMQUIST JK, GRIFFIN JD & SAPER CB 1996a Ventromedial preoptic prostaglandin E2 activates fever-producing autonomic pathways. J Neurosci, 16, 6246–54. [PubMed: 8815905]

SCAMMELL TE, ELMQUIST JK, GRIFFIN JD & SAPER CB 1996b Ventromedial preoptic prostaglandin E2 activates fever-producing autonomic pathways. Journal of Neuroscience, 16, 6246–6254. [PubMed: 8815905]

SCAMMELL TE, GRIFFIN JD, ELMQUIST JK & SAPER CB 1998 Microinjection of a cyclooxygenase inhibitor into the anteroventral preoptic region attenuates LPS fever. American Journal of Physiology-Regulatory Integrative and Comparative Physiology, 274, R783–R789.

SCHULZ TJ, HUANG TL, TRAN TT, ZHANG H, TOWNSEND KL, SHADRACH JL, CERLETTI M, MCDOUGALL LE, GIORGADZE N, TCHKONIA T, et al. 2011 Identification of inducible brown adipocyte progenitors residing in skeletal muscle and white fat. Proc Natl Acad Sci U S A, 108, 143–8. [PubMed: 21173238]

SHIOW LR, FAVRAIS G, SCHIRMER L, SCHANG AL, CIPRIANI S, ANDRES C, WRIGHT JN, NOBUTA H, FLEISS B, GRESSENS P et al. 2017 Reactive astrocyte COX2-PGE2 production inhibits oligodendrocyte maturation in neonatal white matter injury. Glia, 65, 2024–2037. [PubMed: 28856805]

SOLANKI S, DUBE PR, BIRNBAUMER L & VAZQUEZ G 2017 Reduced Necrosis and Content of Apoptotic M1 Macrophages in Advanced Atherosclerotic Plaques of Mice With Macrophage-Specific Loss of Trpc3. Scientific Reports, 7.

SWOAP SJ 2008 The pharmacology and molecular mechanisms underlying temperature regulation and torpor. Biochem Pharmacol, 76, 817–24. [PubMed: 18644349]

THOMAS M, SING H, BELENKY G, HOLCOMB H, MAYBERG H, DANNALS R, WAGNER H, THORNE D, POPP K, ROWLAND L, et al. 2000 Neural basis of alertness and cognitive performance impairments during sleepiness. I. Effects of 24 h of sleep deprivation on waking human regional brain activity. J Sleep Res, 9, 335–52. [PubMed: 11123521]

VALENCIANO AI, CORROCHANO S, DE PABLO F, DE LA VILLA P & DE LA ROSA EJ 2006 Proinsulin/insulin is synthesized locally and prevents caspase- and cathepsin-mediated cell death in the embryonic mouse retina. J Neurochem, 99, 524–36. [PubMed: 17029604]

VASILACHE AM, ANDERSSON J & NILSBERTH C 2007 Expression of PGE(2) EP3 receptor subtypes in the mouse preoptic region. Neuroscience Letters, 423, 179–183. [PubMed: 17706357]

VIRTANEN KA, LIDELL ME, ORAVA J, HEGLIND M, WESTERGREN R, NIEMI T, TAITTONEN M, LAINE J, SAVISTO NJ, ENERBACK S et al. 2009 Functional brown adipose tissue in healthy adults. N Engl J Med, 360, 1518–25. [PubMed: 19357407]

VOSSELMAN MJ, BRANS B, VAN DER LANS AA, WIERTS R, VAN BAAK MA, MOTTAGHY FM, SCHRAUWEN P & VAN MARKEN LICHTENBELT WD 2013 Brown adipose tissue activity after a high-calorie meal in humans. Am J Clin Nutr, 98, 57–64. [PubMed: 23719558]

WANG B, LI A, LI X, HO PW, WU D, WANG X, LIU Z, WU KK, YAU SS, XU A et al. 2018 Activation of hypothalamic RIP-Cre neurons promotes beiging of WAT via sympathetic nervous system. EMBO Rep, 19.

WANG Y, HSUCHOU H, HE Y, KASTIN AJ & PAN W 2015 Role of Astrocytes in Leptin Signaling. J Mol Neurosci, 56, 829–839. [PubMed: 25687329]

WU GY, DEISSEROTH K & TSIEN RW 2001 Spaced stimuli stabilize MAPK pathway activation and its effects on dendritic morphology. Nat Neurosci, 4, 151–8. [PubMed: 11175875]

XU J, CHALIMONIUK M, SHU Y, SIMONYI A, SUN AY, GONZALEZ FA, WEISMAN GA, WOOD WG & SUN GY 2003 Prostaglandin E2 production in astrocytes: regulation by cytokines,

extracellular ATP, and oxidative agents. Prostaglandins Leukot Essent Fatty Acids, 69, 437–48. [PubMed: 14623498]

YANG L, QI Y & YANG Y 2015 Astrocytes control food intake by inhibiting AGRP neuron activity via adenosine A1 receptors. Cell Rep, 11, 798–807. [PubMed: 25921535]

YOSHIDA K, LI XD, CANO G, LAZARUS M & SAPER CB 2009 Parallel Preoptic Pathways for Thermoregulation. Journal of Neuroscience, 29, 11954–11964. [PubMed: 19776281]

YUN CH, KIM JG, PARK BS, LEE HM, KIM DH, KIM EO, PARK JJ, PARK JW, DAMANTE G, KIM YI et al. 2011 TTF-1 action on the transcriptional regulation of cyclooxygenase-2 gene in the rat brain. PLoS One, 6, e28959. [PubMed: 22174936]

Author Manuscript

Author Manuscript

Author Manuscript

Author Manuscript
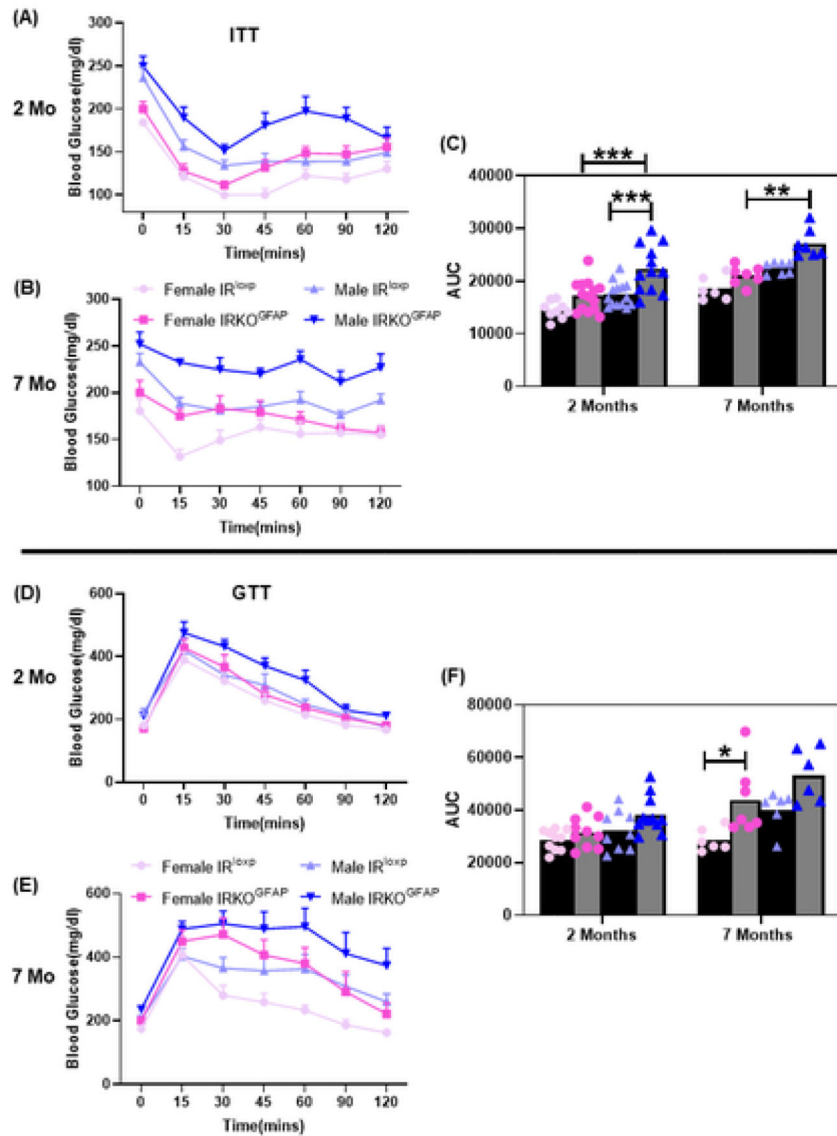
Figure 1. IRKO^GFAP mice exhibit sex differences in insulin sensitivity and glucose tolerance over time.

(**A**) Insulin tolerance test (ITT) measurements of blood glucose levels for females (n=9–14 per group) and males (n=9–13 per group) after peripheral insulin injections (0.75U/kg IP) at 2 months of age. (**B**) ITT measurements of blood glucose levels for females (n= 6–8 per group) and males (n=7 per group) after peripheral insulin injections at 7 months of age. (**C**) Area under curve (AUC) measurements of ITT for females and males at 2 months and 7 months of age. (**D**) Glucose tolerance test (GTT) measurements of blood glucose levels for females (n=10 per group) and males (n=9–11 per group) after peripheral glucose injection (2g/kg) at 2 months of age. (**E**) GTT measurements of blood glucose levels for females (n=6–8 per group) and males (n=7 per group) after peripheral glucose injection at 7 months of age. (**F**) Area under curve (AUC) measurements of GTT for females and males at 2 months and 7 months of age. The female IR^loxp group is represented with light pink line/dots, female IRKO^GFAP group with dark pink line/dots, male IR^loxp group with light blue

line/dots and male IRKO^{GFAP} group with dark blue line/dots. Values are expressed as means ± SEM. * P<0.0332, * * P<0.0021, *** P<0.0002, **** P< 0.0001 by three-way ANOVA and Tukey post-hoc test relative to IRKO^{GFAP} versus IR^{loxp} groups.
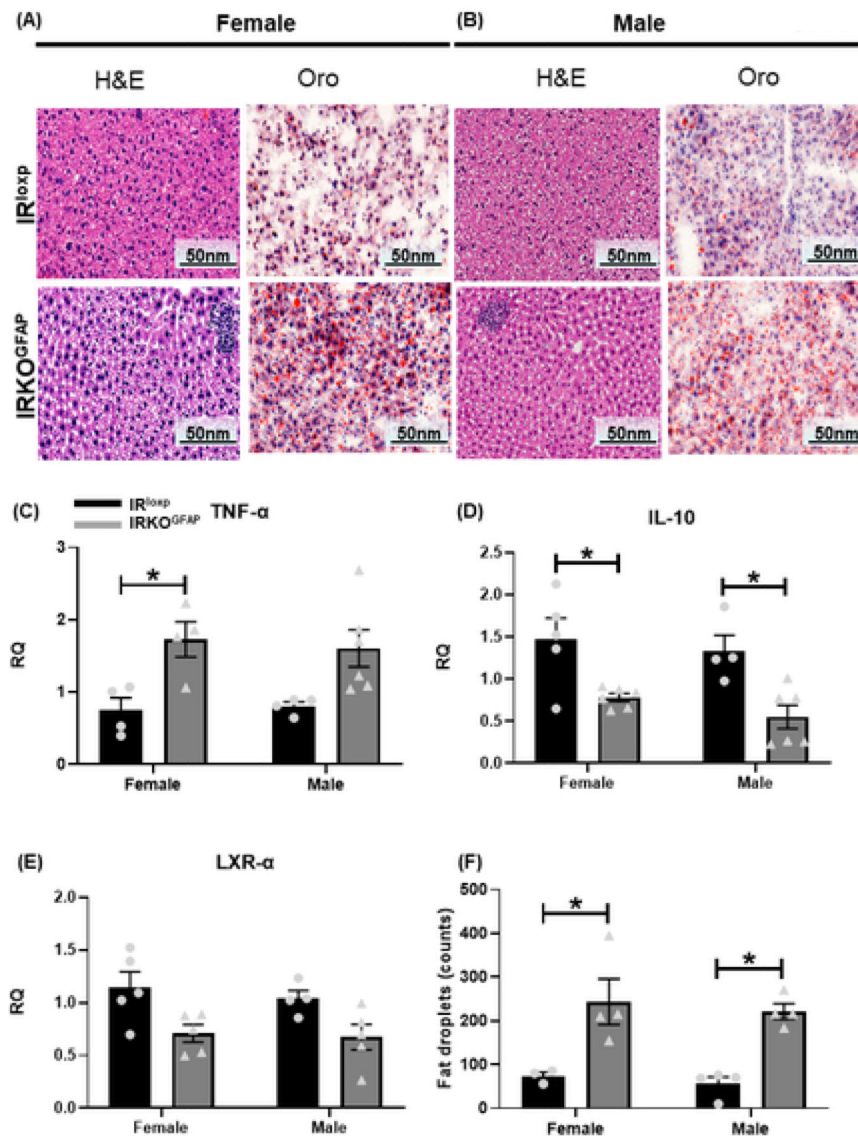
Figure 2. IRKO^{GFAP} mice exhibit alterations in liver morphology and inflammation at 7–8 months of age.
(A-B) Histological H&E and ORO analysis of liver sections in females (n=3–4 per group) and males (n=4 per group). **(C)** Quantification of RT-PCR data showing fold change (RQ=2^{-} ^{Ct}) in TNF-α mRNA expression in female and male mice (n=4 for females and 4–6 for males). **(D)** Quantification of RT-PCR data showing fold change in IL-10 mRNA levels in females and males (n=4–5 for females and 4–6 for males). **(E)** Quantification of RT-PCR data showing fold change in LXR- α mRNA expression in females and males (n=5 for females and 4–5 for males). **(F)** Quantitative analysis of fat droplets in liver tissues of female and males mice (n=3 per group). Female IR^{loxp} group is represented with black bar/circle dots, female IRKO^{GFAP} group with dark grey bar/triangle dots, male IR^{loxp} group with black bar/circle dots and male IRKO^{GFAP} group with dark grey bar/triangle dots. Values are expressed as means ± SEM. * $P<0.0332$, * * $P<0.0021$, *** $P<0.0002$, **** $P< 0.0001$ by two-way ANOVA and Tukey post-hoc test relative to IRKO^{GFAP} versus IR^{loxp} groups.
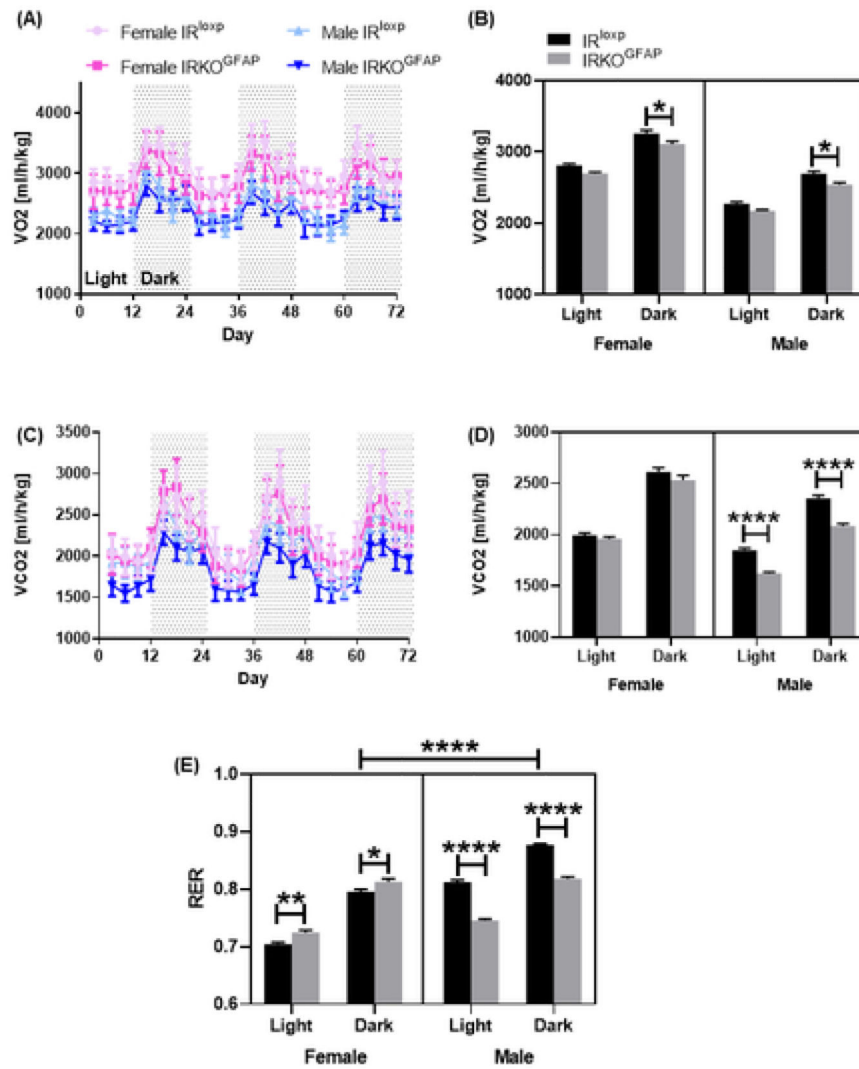
Figure 3. At 7–8 months of age, IRKO^{GFAP} mice display significant sex differences in energy utilization.

IRKO^{GFAP} mice were fed *ad libitum* and subjected to indirect calorimetry analysis to assess light and dark cycle of **(A)** O_2 consumption in females and males, **(B)** carbon dioxide production (VCO_2) in females and males and **(C)** respiratory exchange ratio (RER) in female and male mice. Values represent measurements of 3 consecutive days. n=4 per group. The female IR^{loxp} group is represented with a light pink line/black bar, the female IRKO^{GFAP} group with a dark pink line/grey bar, the male IR^{loxp} group with a light blue line/ black bar and the male IRKO^{GFAP} group with a dark blue line/grey bar. Values are expressed as means ± SEM. * $P<0.0332$, * * $P<0.0021$, *** $P<0.0002$, **** $P< 0.0001$ by three-way ANOVA and Tukey post-hoc test relative to IRKO^{GFAP} versus IR^{loxp} groups.
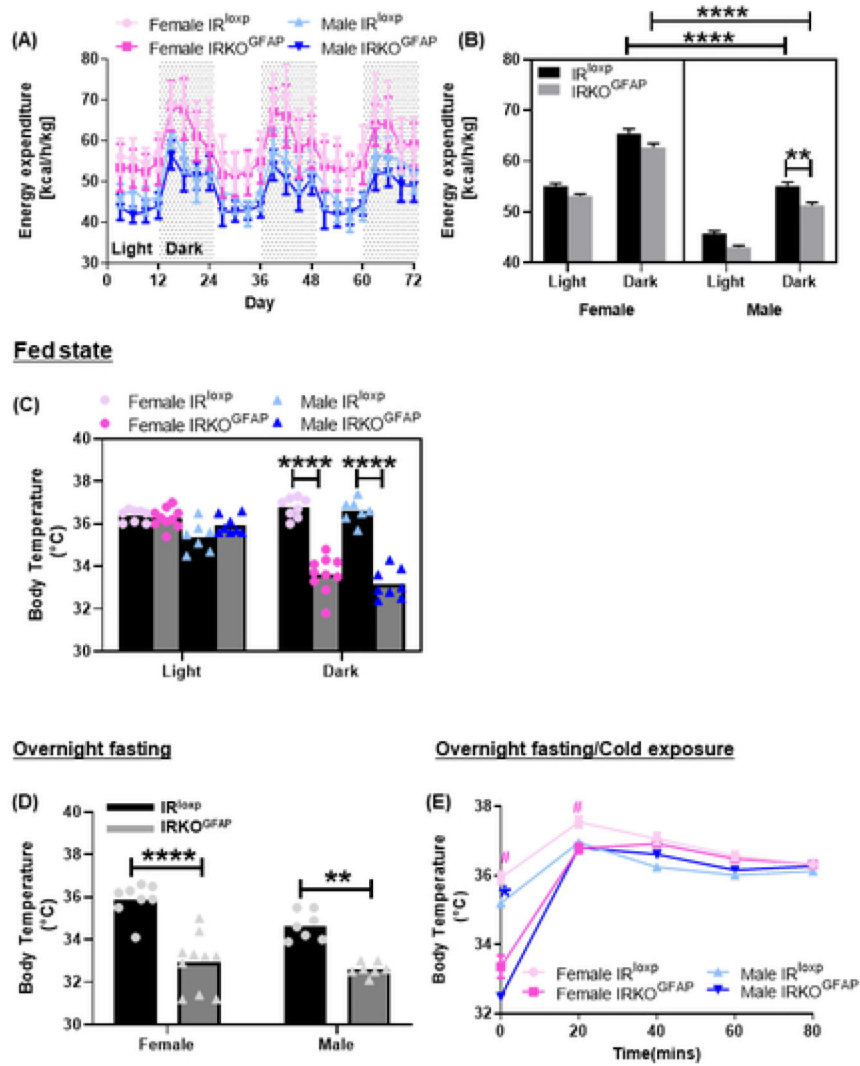
Figure 4. Despite sex differences in energy expenditure, IRKO^{GFAP} mice display a significant reduction in body temperature at 9 months of age.

IRKO^{GFAP} mice were fed *ad libitum* and subjected to indirect calorimetry analysis to assess light and dark cycle of **(A)** energy expenditure for three consecutive days for female and male mice (n=4 per group). Recording of body temperature measurements via rectal probe in females and males during **(B)** fed state, **(C)** overnight fasting, and **(D)** overnight fasting/ cold exposure condition. n= 8–10 per group for females, n=7–8 per group for males. The female IR^{loxp} group is represented with a light pink line/black bar, the female IRKO^{GFAP} group with a dark pink line/grey bar, the male IR^{loxp} group with a light blue line/black bar and the male IRKO^{GFAP} group with a dark blue line/grey bar. Values are expressed as means ± SEM. * P<0.0332, * * P<0.0021, *** P<0.0002, **** P< 0.0001 by two-way ANOVA and Tukey post-hoc test (panel D) and three-way ANOVA and Tukey post-hoc test relative to IRKO^{GFAP} versus IR^{loxp} groups.
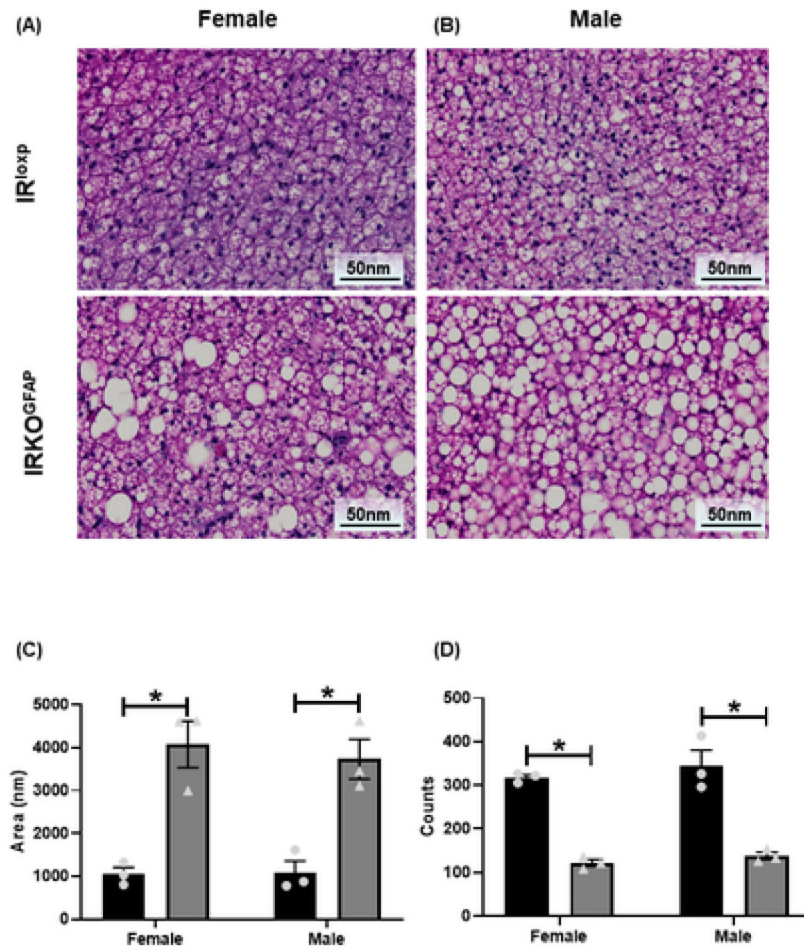
Figure 5. IRKO^{GFAP} mice show alterations in BAT morphology and larger droplet size at 9 months of age.

(A-B) Histological H&E analysis in females and males. (C) Quantitative analysis of fat droplet area in female and male mice. (D) Quantification of BAT cell counts in females and males. n=3 per group. Female IR^{loxp} group is represented with black bar/circle dots, female IRKO^{GFAP} group with dark grey bar/triangle dots, male IR^{loxp} group with black bar/circle dots and male IRKO^{GFAP} group with dark grey bar/triangle dots. Values are expressed as means ± SEM. * $P<0.0332$, * * $P<0.0021$, *** $P<0.0002$, **** $P< 0.0001$ by two-way ANOVA and Tukey post-hoc test relative to IRKO^{GFAP} versus IR^{loxp} groups.
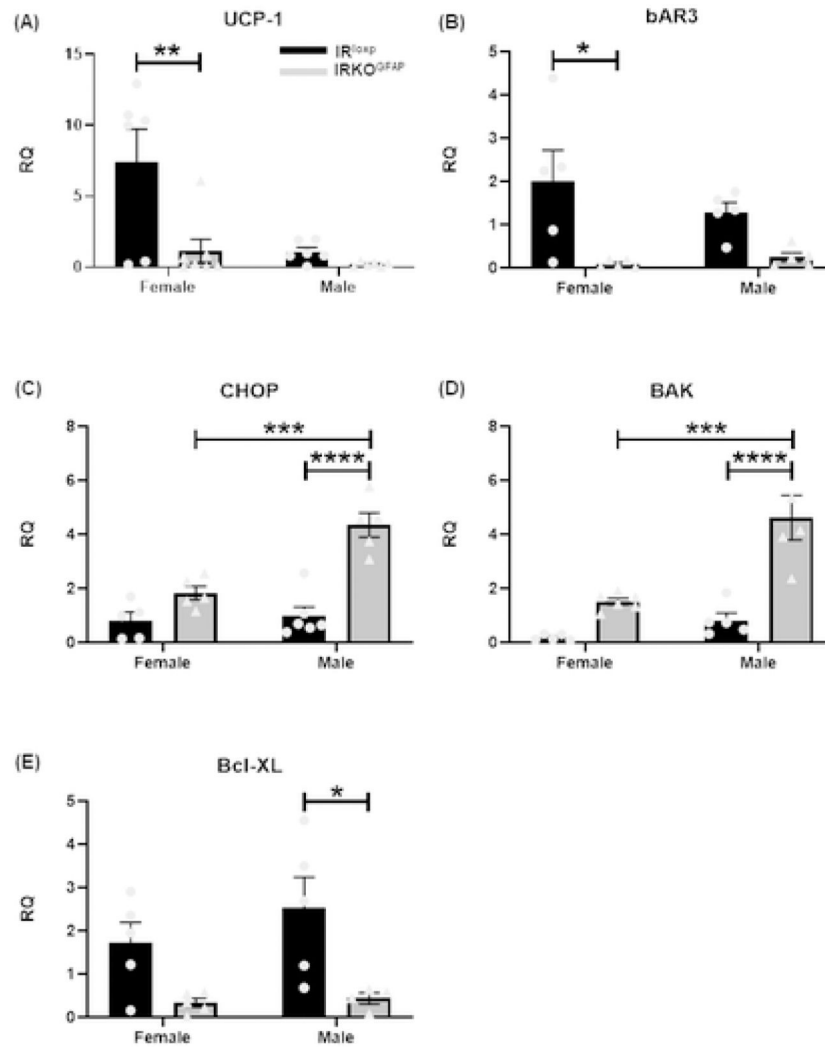
Figure 6. At 9 months of age, IRKO$^{\text{GFAP}}$ BAT exhibit sex differences in gene expression that are consistent with lower thermogenesis and higher apoptosis.

Quantification of RT-PCR data showing fold change (RQ=2$^{-\Delta\Delta Ct}$) in **(A)** UCP-1 mRNA levels, **(B)** βAR3 mRNA levels, **(C)** pro-apoptotic marker CHOP mRNA levels, **(D)** pro-apoptotic BAK mRNA levels, and **(E)** Anti-apoptotic Bcl-XL mRNA levels in female and male BAT tissues. (n=4–7 per group). The female IR$^{\text{loxp}}$ group is represented with black bar/circle dots, the female IRKO$^{\text{GFAP}}$ group with dark grey bar/triangle dots, the male IR$^{\text{loxp}}$ group with black bar/circle dots and the male IRKO$^{\text{GFAP}}$ group with dark grey bar/triangle dots. Values are expressed as means ± SEM. * P<0.0332, * * P<0.0021, *** P<0.0002, **** P< 0.0001 by two-way ANOVA and Tukey post-hoc test relative to IRKO$^{\text{GFAP}}$ versus IR$^{\text{loxp}}$ groups.
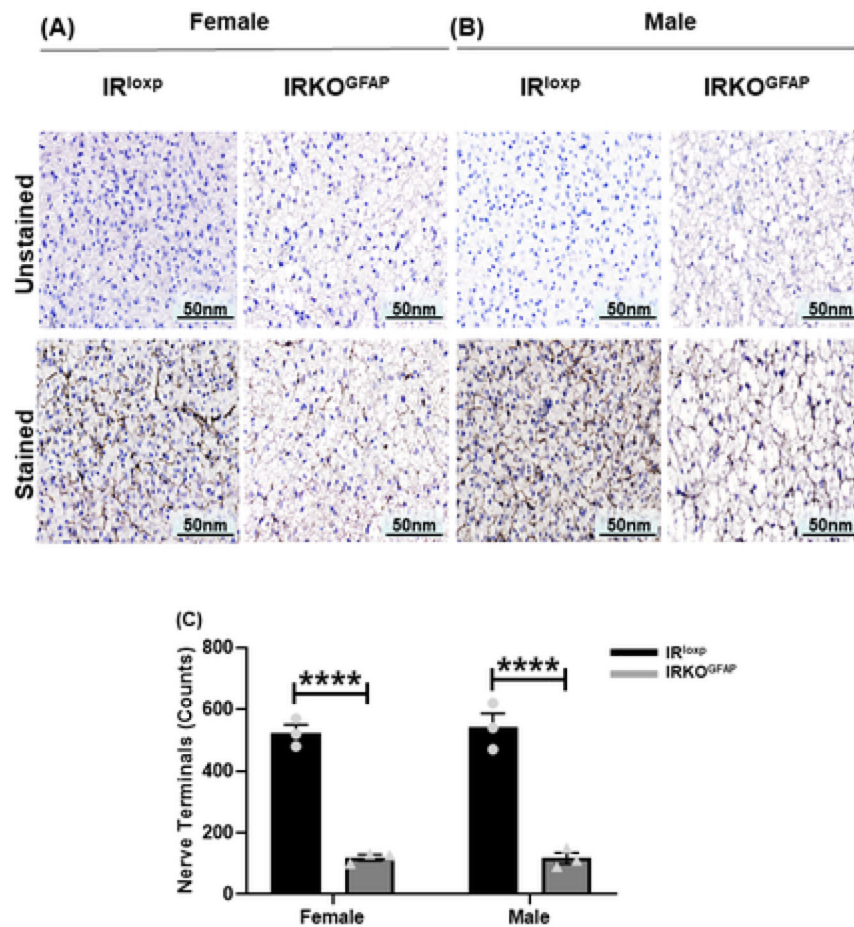
Figure 7. IRKO^{GFAP} mice show less innervation of BAT tissue at 9–10 months of age

(A-B) Representative images of immunohistochemical (IHC) sections of unstained and stained tyrosine hydroxylase (TH) in BAT tissues of females and males. **(C)** Quantitative analysis of positive nerve terminals in females and males. n=3 per group. The female IR^{loxp} group is represented with a black bar/circle dots, the female IRKO^{GFAP} group with dark a grey bar/triangle dots, the male IR^{loxp} group with a black bar/circle dots and the male IRKO^{GFAP} group with a dark grey bar/triangle dots. Values are expressed as means ± SEM. * P<0.0332, * * P<0.0021, *** P<0.0002, **** P< 0.0001 by two-way ANOVA and Tukey post-hoc test relative to IRKO^{GFAP} versus IR^{loxp} groups.
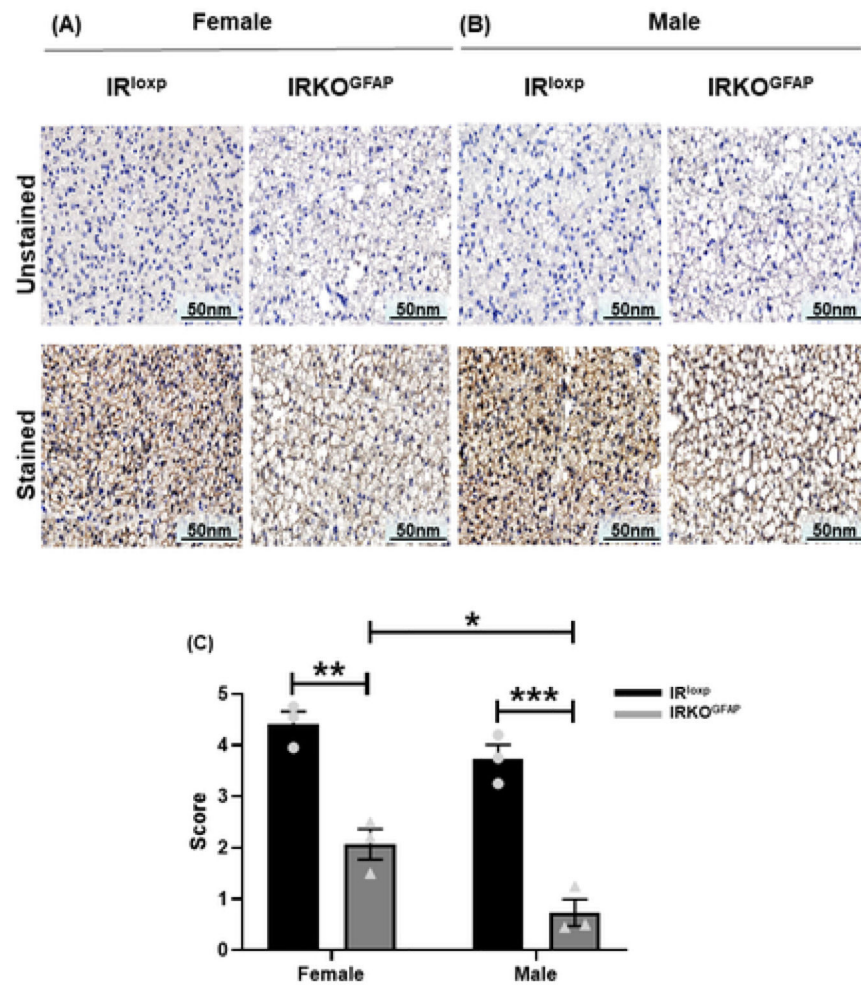
Figure 8. At 9–10 months of age, IRKO^{GFAP} mice show lower β-adrenergic receptor 3 levels in BAT tissues.

(A-B) Representative images of immunohistochemical (IHC) sections of unstained and stained βAR3 density of BAT tissues in females and males. **(C)** Quantification of the density of browning with a score from 1 (lowest intensity) to 5 (highest intensity) in female and male mice. n=3 per group. The female IR^{loxp} group is represented with a black bar/circle dots, the female IRKO^{GFAP} group with a dark grey bar/triangle dots, the male IR^{loxp} group with a black bar/circle dots and the male IRKO^{GFAP} group with a dark grey bar/triangle dots. Values are expressed as means ± SEM. * $P<0.0332$, * * $P<0.0021$, *** $P<0.0002$, **** $P<0.0001$ by two-way ANOVA and Tukey post-hoc test relative to IRKO^{GFAP} versus IR^{loxp} groups.